actuators

MDPI

Article

Mechanical Design of a New Hybrid 3R-DoF Bioinspired Robotic Fin Based on Kinematics Modeling and Analysis

Eliseo de J. Cortés Torres *,†, Luis E. García Gonzales, Luis E. Villamizar Marin and Cecilia E. García Cena

Escuela Técnica Superior de Ingeniería y Diseño Industrial, Centre for Automation and Robotics (UPM-CSIC), Universidad Politécnica de Madrid, Ronda de Valencia, 3, 28012 Madrid, Spain; le.garcia@alumnos.upm.es (L.E.G.G.); luis.villamizar@alumnos.upm.es (L.E.V.M.); cecilia.garcia@upm.es (C.E.G.C.)

* Correspondence: eliseo.cortes@alumnos.upm.es

† Current address: Ronda de Valencia, 3, 28012 Madrid, Spain.

Abstract: The field of bioinspired underwater robots aims to replicate the capabilities of marine animals in artificial systems. Stingrays have emerged as highly promising species to be mimicked because of their flat body morphology and size. Furthermore, they are considered high-performance species due to their maneuverability, propulsion mode, and sliding efficiency. Designing and developing mechanisms to imitate their pectoral fins is a challenge for underwater robotic researchers mainly because the locomotion characteristics depend on the coordinated movement of the fins. In the state of the art, several mechanisms were proposed with 2 active rotation degrees of freedom (DoFs) to replicate fin movement. In this paper, we propose adding an additional active DoF in order to improve the realism in the robotic manta ray movement. Therefore, in this article, we present the mechanical design, modeling, and kinematics analysis of a 3-active-and-rotational-DoF pectoral fin inspired by the *Mobula Alfredi* or reef manta ray. Additionally, by using the kinematics model, we were able to simulate and compare the behaviour of both mechanisms, that is, those with 2 and 3 DoFs. Our simulation results reveal an improvement in the locomotion, and we hypothesized that with the third DoF, some specific missions, such as hovering or fast emergence to the surface, will have a better performance.

Keywords: bioinspired; compliant joints; underwater robots

Citation: Cortés Torres, E.d.J.; García Gonzales, L.E.; Villamizar Marin, L.E.; García Cena, C.E. Mechanical Design of a New Hybrid 3R-DoF Bioinspired Robotic Fin Based on Kinematics Modeling and Analysis. *Actuators* **2024**, *13*, 353. https://doi.org/10.3390/act13090353

Academic Editor: Zhuming Bi

Received: 10 August 2024
Revised: 8 September 2024
Accepted: 9 September 2024
Published: 11 September 2024

1. Introduction

For millions of years, different species have evolved in such a way that they have adapted to the diverse conditions of their environment, with an example being fish and marine animals, which have developed behavioral, physiological, and morphological adaptations to face the conditions of the marine environment, specifically the temperature, salinity, pH, oxygen and carbon dioxide contents of the water, and pressure, among others, which, in many cases, can become extreme [1]. Numerous researchers have been interested in studying these adaptations in order to understand natural behaviour and describe the hydrodynamic principles that drive them. This knowledge has been used in various applications, including bioinspired underwater robotics.

Biologically inspired underwater vehicles are designed by imitating the characteristics of marine species, such as their high-efficiency capabilities [2]. Batoid fish, including stingrays, are considered high-performance species due to their maneuverability and thrust production, allowing them to leap out of the water and reach speeds close to 2.8 m/s with low frequencies of flapping and undulating. Thanks to these characteristics, they can migrate over long distances, populate underwater regions, and even descend to depths of around 1400 m [3,4]. Furthermore, their flat body and large size can be replicated to enhance the payload capability, and their pectoral fins can offer vectored propulsion, providing

great sliding efficiency typical of median and paired pectoral fin (MPF) mode, allowing them to travel long distances without resting [5–7].

Given the aforementioned characteristics, numerous research groups have developed underwater vehicles inspired by stingrays [6,8,9]. Furthermore, several studies have focused on important aspects such as the hydrodynamics of stingrays [10] to better understand the locomotion of these species, as well as the use of different materials for their construction [11–14], including the use of actuators with smart materials, such as shape memory alloy wire (SMA) [15,16]. However, the main emphasis lies in the development of suitable mechanisms to improve realism in robotic fin locomotion. The MFP swim is characterized by maneuverability and stability. For vehicles inspired by stingrays, it is essential to use mechanisms capable of executing oscillating movements of the pectoral fins and achieving adequate propulsion. Mechanisms have been developed based on propulsion speed, thrust, and robot power, presenting different configurations with controllable parameters, namely frequency, amplitude, wavelength, fin shape, and undulatory mode [17]. Some of the developed configurations include a radial scissor mechanism with only one actuator per fin [18], a propulsion mechanism with undulating fins with multiple actuators [19], a rocking crank mechanism [20], and flexible beam mechanisms achievable by implementing metal cables and rigid bones [21], among others.

In the case of stingrays, the muscles of the fins are thicker, while those at the basal part are stronger, generating greater driving power. In the distal part, there is more cartilage and soft tissue, which serve as controllers to adjust the wave transfer on the fin surface. In [5], a pectoral fin module is proposed with a 2 DoF spatial parallel mechanism (SPM) that mimics these characteristics.

Morphology Selection

Among the Mobula species, there exist different specimens that could be used as inspiration for designing underwater robots, including devil manta rays, reef manta rays, and giant manta rays. According to [22], most of them live in the world's extensive water areas, which helps with integrating the robot into the environment. Manta rays' glider shape offers different advantages; for instance, some Mobula alfredi specimens can reach a wingspan of 8.8 m [23]. This characteristic is considered as a strength in the selection of this type of animal, and the size of its body is suitable for the integration of mechatronics elements. Indeed, small objects in the ocean are difficult to identify, but the manta ray shape is suited to stealth tasks. Furthermore, the natural flexibility of the manta ray fins and its glider shape also help to facilitate greater manoeuvrability in small spaces. Additionally, these marine animals can navigate over 450 m of depth, another characteristic making their morphology suitable for underwater robot applications.

Based on previous considerations, we considered the morphology of a manta ray (Mobula Alfredi) as the baseline for the mechanical design of our bioinspired underwater robot.

Other authors have also considered a manta ray morphology. Perhaps the mechanism proposed by [5] is the closest to our mechanism. However, in [5], the locomotion pattern is generated by the SPM placed near to the fin base. These authors suggested that an additional DoF could improve the behaviour of the fin, making it more natural. In [21,24], the authors proposed different mechanisms for the fin, wherein the SPM was replaced by a fin designed under cantilever beam principles.

In this paper, we analyze the impact of the third DoF in terms of movement amplitude and power consumption by modeling an entire mechanism and simulating it under different scenarios.

According to the evidence provided by our theoretical study, we decided to include an additional DoF in the mechanical design. Additionally, in this article, we present a prototype of a new hybrid pectoral robotic fin based on a Mobula Aldredi manta ray with 3 active rotational DoFs. Despite, the third degree of freedom introducing additional complexity in kinematic modeling, the hypothesis is that it could reduce the power consumption while

improving the performance and efficiency of the navigation by making the movement more natural. In addition, the manoeuvrability could be improved due to this third DoF, mainly targeting manoeuvrability in narrow spaces. We have also compared the strengths and weaknesses of both morphologies, that is, those with 2 and 3 DoFs, in order to validate the hypothesis that an additional DoF improves the navigation capabilities of a bioinspired fin, and in some missions, hovering could be optimized by using this extra DoF. Figure 1a shows a model sketch using the manta ray as a background for design.

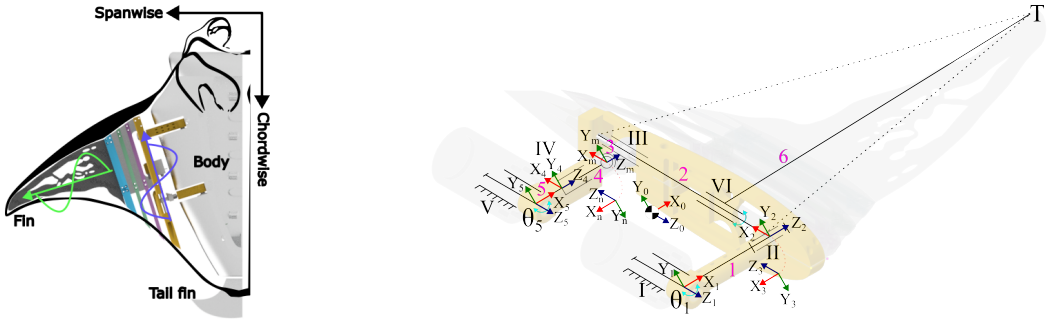

(**a**) (**b**)

Figure 1. The 3 DoF robotic fin mechanism and the scheme for the kinematics model: (**a**) hybrid mechanism coupled with a background representation of a manta ray (Mobula Alfredi) and (**b**) spatial hybrid mechanism representation with the 3 DoFs, where joints I, V, and VI are active, while joints II, III, and IV are passive.

This document is organized as follows: Sections 2 and 3 present the analysis and simulation of the kinematic model of the mechanism with 2 and 3 DoFs, and finally, Section 4 presents the mechanical design.

2. Kinematic Analysis

Figure 1b presents the configuration of the spatial hybrid mechanism with 3 active degrees of freedom. Furthermore, the figure shows the local reference systems associated with each joint.

Using a Lie algebra methodology, the entire mechanism is split up; then, it can be analyzed by considering two subsystems, with one of them involving the spatial mechanism, S_0 to S_6, with 2 DoFs, and the other involving the 1 DoF serial mechanism described by S_6 to S_{T_f}. In the following subsections, each subsystem is mathematically modeled.

2.1. Two-Degrees of Freedom Spatial Mechanism Direct Kinematics

The method used to analyze the joint localization of the mechanism is based on the Lie algebra method and is extensively explained in [25]. Therefore, an *i*th coordinate system is created on each *i*th body, aiming to describe its position with respect to a global system $\{S_0\}$. This approach suggests the transformation of close-loop mechanisms into open-loop mechanisms restricted for the position and orientation in a common joint where all the kinematic chains converge [25]. Thus, it is possible to define two vectors, one for the active joints (Equation (1)), and the other for the passive joints (Equation (2))

$$\theta_{act} = [\theta_5, \theta_1], \tag{1}$$

$$\theta_{pas} = [d_{z4}, \theta_2, d_{z3}]. \tag{2}$$

where θ_i and d_{zi} are the variables associated with the rotational and prismatic joints, respectively. In order to transform the close-loop mechanisms into open loop mechanisms, the proposed method is applied to the spherical joint at the intersection of the rotational coordinate systems $\{S_m\}$ and $\{S_n\}$ (see Figure 1b). Therefore, the spherical joint is decoupled in two kinematic chains, the first one between the systems $\{x_0, y_0, z_0\}$ to $\{x_m, y_m, z_m\}$,

and the second between the systems $\{x_0, y_0, z_0\}$ to $\{x_n, y_n, z_n\}$. As a result, a homogeneous transformation matrix (HTM) is made between $\{x_0, y_0, z_0\}$ and $\{x_5, y_5, z_5\}$:

$$T_{0,5} = \begin{bmatrix} I & r_{CM} \\ 0 & 1 \end{bmatrix} \begin{bmatrix} R_z(\theta_5) & 0 \\ 0 & 1 \end{bmatrix} \tag{3}$$

where $r_{CM} \in R^{3\times1}$ is the position vector between a global position (CM) and the S_1 and S_5. For the systems $\{x_5, y_5, z_5\}$ and $\{x_4, y_4, z_4\}$, the HTM will be as follows:

$$T_{5,4} = \begin{bmatrix} R_y(\pi/2) & 0 \\ 0 & 1 \end{bmatrix} \begin{bmatrix} I & r_z(l_5 + d_{z4}) \\ 0 & 1 \end{bmatrix} \tag{4}$$

where r_z is the position vector cylindrical joint in $\{S_{4,5}\}$. For the systems, $\{x_4, y_4, z_4\}$ and $\{x_m, y_m, z_m\}$

$$T_{4,m} = \begin{bmatrix} I & r_z(l_4) \\ 0 & 1 \end{bmatrix} \tag{5}$$

On the other hand, the second kinematic chain relates the reference systems between $\{x_0, y_0, z_0\}$ and $\{x_n, y_n, z_n\}$. Then, for the first system between $\{x_0, y_0, z_0\}$ and $\{x_1, y_1, z_1\}$, the homogeneous transformation matrix is given by:

$$T_{0,1} = \begin{bmatrix} I & r_{CM} \\ 0 & 1 \end{bmatrix} \begin{bmatrix} R_z(\theta_1) & 0 \\ 0 & 1 \end{bmatrix} \tag{6}$$

Between the reference systems $\{x_1, y_1, z_1\}$ and $\{x_2, y_2, z_2\}$ and for $\{x_2, y_2, z_2\}$ and $\{x_3, y_3, z_3\}$, the transformations are defined by Equation (7) and Equation (8), respectively;

$$T_{1,2} = \begin{bmatrix} I & r_x(l_1) \\ 0 & 1 \end{bmatrix} \begin{bmatrix} R_y(\pi/2) & 0 \\ 0 & 1 \end{bmatrix} \begin{bmatrix} R_z(\theta_2) & 0 \\ 0 & 1 \end{bmatrix} \tag{7}$$

where r_x is the position vector between joints 1 and 2 in $\{S_{1,2}\}$. For the system between,

$$T_{2,3} = \begin{bmatrix} R_y(\pi/2) & 0 \\ 0 & 1 \end{bmatrix} \begin{bmatrix} I & r_z(l_2 + d_{z3}) \\ 0 & 1 \end{bmatrix} \tag{8}$$

Finally, between $\{x_3, y_3, z_3\}$ and $\{x_n, y_n, z_n\}$,

$$T_{3,n} = \begin{bmatrix} I & r_x(l_3) \\ 0 & 1 \end{bmatrix} \tag{9}$$

2.1.1. Constraint Vector

The behavior of the mechanism is described by the position analysis of the spherical joint and by the physical constraints in the joint that has been decoupled. Spherical joints have 3 DoFs related to the rotation in each axis. The constraints are related to the linear displacement in the three axes and are described in the following equation:

$$\Phi = \begin{bmatrix} R_{0,n} u_{x,x} (r_n - r_m) \\ R_{0,n} u_{y,y} (r_n - r_m) \\ R_{0,n} u_{z,z} (r_n - r_m) \end{bmatrix} \tag{10}$$

where $u_{x,x}, u_{y,y}, u_{z,z}$ are unit vectors associated with the local axis in each joint, while $(r_n - r_m)$ is the difference in position between the systems $\{x_n, y_n, z_n\}$ and $\{x_m, y_m, z_m\}$, since we have a base system view.

2.1.2. Jacobian Matrix

The constraint vector time derivative is given by $\dot{\Phi} = \Phi_\theta \dot{\theta}_j$, which can be expressed in Lie algebra terms as:

$$\Phi_\theta(j,i) = C^T_{nj,nj} Ad_{Tnj,i} S_i \tag{11}$$

Here, S_i is an element of the Lie algebra $se(3)$, which describes the velocity of the ith joint. The covector $C^T_{nj,nj}$ represents the reaction force (wrench) at the decoupled joint, while $AdTnj, i$ is the adjoint matrix, which represents the action of the Lie group $SE(3)$ on its Lie algebra $se(3)$. In general terms, the components $C^T nj, njAdTnj, iS_i$ describe the relationship between the jth constraint and the ith joint's DoF, and $\dot{\theta}_i$ represents the joint velocity values. Thus, the twist described for the Jacobian (Φ_θ) of each passive and active joint can be expressed by:

$$\begin{aligned} S_{rot} &= [0,0,1,0,0,0] \\ S_{trans} &= [0,0,0,0,0,1] \end{aligned} \tag{12}$$

where $\{S_{rot}\}$ represents the twist description for the rotational joints, that, is axes $\{S_2\}$, $\{S_4\}$ and $\{S_5\}$, while $\{S_{trans}\}$ represents the twist for the prismatic joints, that is, $\{S_3\}$ and $\{S_6\}$. Finally, the Jacobian is given by,

$$\Phi_\theta(:,1:2) = \begin{bmatrix} -C^T_x Ad_{Tn,m} Ad_{Tm,5} S_5 & -C^T_x Ad_{Tn,m} Ad_{Tm,4} S_4 \\ -C^T_y Ad_{Tn,m} Ad_{Tm,5} S_5 & -C^T_y Ad_{Tn,m} Ad_{Tm,4} S_4 \\ -C^T_z Ad_{Tn,m} Ad_{Tm,5} S_5 & -C^T_z Ad_{Tn,m} Ad_{Tm,4} S_4 \end{bmatrix}$$

$$\Phi_\theta(:,3:5) = \begin{bmatrix} C^T_x Ad_{Tn,1} S_1 & C^T_x Ad_{Tn,2} S_2 & C^T_x Ad_{Tn,3} S_3 \\ C^T_y Ad_{Tn,1} S_1 & C^T_y Ad_{Tn,2} S_2 & C^T_y Ad_{Tn,3} S_3 \\ C^T_z Ad_{Tn,1} S_1 & C^T_z Ad_{Tn,2} S_2 & C^T_z Ad_{Tn,3} S_3 \end{bmatrix}$$

The Jacobian can be split, taking into account the passive and active joints, as follows:

$$\Phi_{\theta act} = [\Phi_\theta(:,1), \Phi_\theta(:,3)] \tag{13}$$

$$\Phi_{\theta pas} = [\Phi_\theta(:,2), \Phi_\theta(:,5), \Phi_\theta(:,6)] \tag{14}$$

2.1.3. Position Analysis

The following (Equation (15)) describes the kinematic relation between active and passive joints:

$$\Phi_{\theta act} \Delta\theta_{act} + \Phi_{\theta pas} \Delta\theta_{pas} = -\Phi \tag{15}$$

In the case that the parameters of the active joints are the reference signals for the system, it could be assumed that $\Delta\theta_{act} = 0$. Then, Equation (15) can be rewritten as

$$\Phi_{\theta pas} \Delta\theta_{pas} = -\Phi \tag{16}$$

The Newton–Raphson method was implemented to obtain a numerical solution for Equation (16).

2.2. One-Degree of Freedom Serial Mechanism Direct Kinematics

Due to this mechanism's serial nature, the fin tip (T_f) position can be described by a linear combination of its joints, as shown in Figure 2.

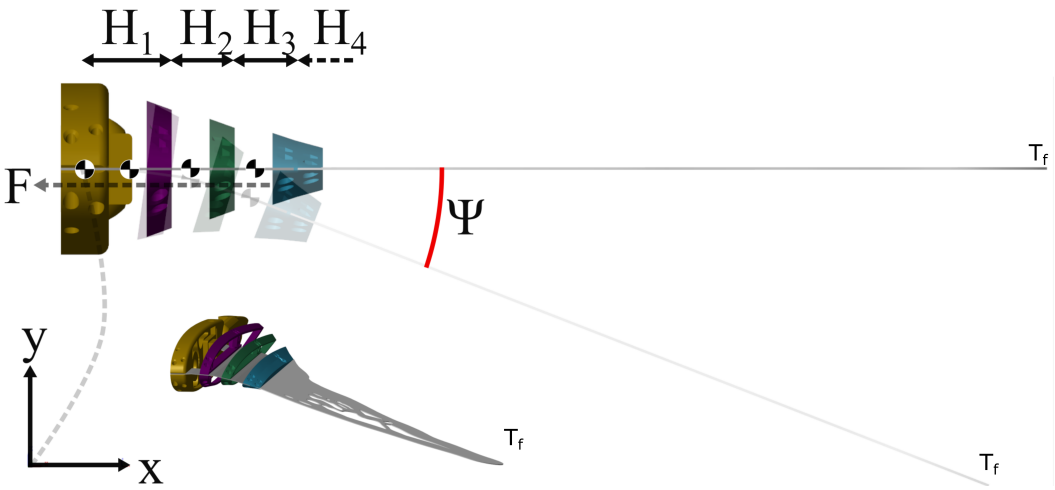

Figure 2. Fin tip location change when a force F is applied, generating a deformation angle Ψ that is considered as the third DoF.

Thus, for a given coordinate system $\{XYZ\}$ located at $\{S_6\}$ and if all joints are considered as rotational (see Figure 2), the position of T_f could be computed by the following

$$\begin{aligned} T_{o-x} &= \sum_{i=1}^{n} H_i cos\left(\frac{i\Psi}{n}\right) \\ T_{o-y} &= \sum_{i=1}^{n} H_i sin\left(\frac{i\Psi}{n}\right) \end{aligned} \quad . \tag{17}$$

where $n = 3$ is the number of passive DoFs of the mechanism, $H \in R^{3\times1}$ is the vector component for each link, and Ψ is the deformation or deflection angle created for the force in the wires. This vector could be described as

$$H = [H_1 ... H_n] \tag{18}$$

2.3. Inverse Kinematics

For the inverse kinematic analysis, the α and β angles are the input values required to compute the inverse kinematics. Moreover, the α angle can be expressed as a function of θ_5 and θ_1 (see Figure 3).

For the spatial mechanism, the parameters α and β can be modeled using the following equations:

$$\alpha(t) = \alpha_{max} Sin(2\pi f t) \tag{19}$$

$$\beta(t) = \beta_{max} Cos(2\pi f t) \tag{20}$$

where f is the frequency of the movement, t is the time domain variable, and β_{max} and α_{max} are related to the mechanism-desired motion, considering their physical constraints. Therefore, β_{max} is the maximum pitching angle, and α_{max} is the maximum flapping amplitude. Considering Figure 3, it is possible to express the α angles as:

$$\alpha(t) = (\theta_1 + \theta_5)/2, \tag{21}$$

and

$$\arctan(l_3/l_1) = \theta_5 - \theta_1 \tag{22}$$

where

$$l_3 = l_0 \tan(\beta(t)) \tag{23}$$

Considering Equations (21) and (22), variables θ_5 and θ_1 could be computed by

$$\theta_5 = (\arctan(l_3/l_1) + 2\alpha)/2 \tag{24}$$

$$\theta_1 = (2\alpha) - \theta_5 \tag{25}$$

Finally, for the serial mechanism,

$$\sum_{i=1}^{n} \frac{i\Psi}{n} = \alpha \tag{26}$$

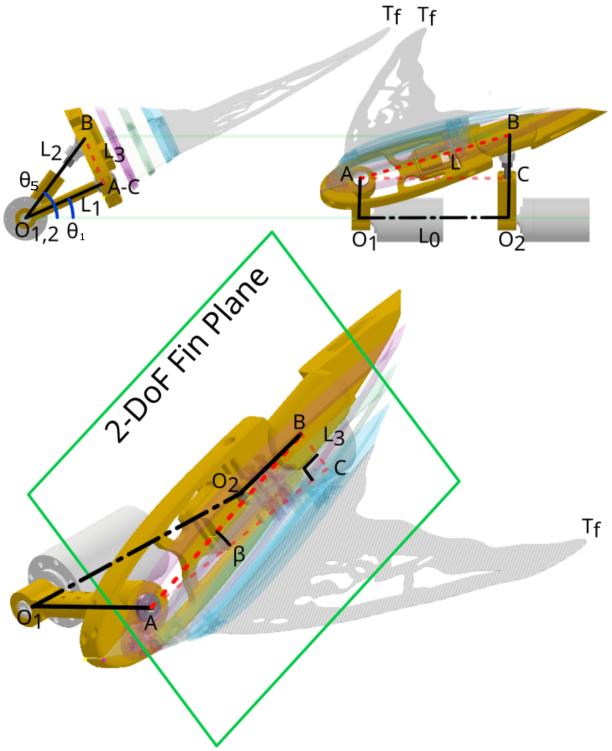

Figure 3. The geometricrelationship parameters considering the mechanism motion plane.

3. Kinematic Analysis Simulation

In this section, we describe how we conducted simulations to analyze whether the additional DoF improves the mobility of the fin.

To facilitate this, we implemented a previous kinematic model into a MatLab environment. Four different scenarios are proposed. In each scenario, the input signal is modified while the extra DoF is switched on and off in order to evaluate the improvements in the movements in terms of amplitude.

For Scenarios 1 and 2, the CPG input signal, according to [5], was implemented. In Scenario 1, the third DoF is switched off, while in Scenario 2, it is switched on. We proceed in a similar way for Scenarios 3 and 4, but in these cases, the input signal is mathematically described by [10] and replicates the natural movements of a manta ray. In Scenario 3, the third DoF is switched off, while in Scenario 4, it is switched on.

Tables 1 and 2 show the physical parameters and mechanical constraints for links and joints according to the mechanical design.

Table 1. Geometric considerations implemented in simulation.

i_{th} Link	Length (mm)
L_1	104
L_5	104
L_2	172

The simulation time is $t = 6.6$ s , and the frequency is $f = 0.15$ Hz. Additionally, the maximum pitching angle is $\beta_{max} = 25°$, and the maximum flapping amplitude is $\alpha_{max} = 60°$.

Table 2. Translational joints' constraint limits.

i_{th} **Joint**	**Max. Displacement (mm)**
d_{z4}	38
d_{z3}	40

3.1. Simulations Using a Sinusoidal CPG Approach

Figure 4a shows the fin mechanism movement, where the point T_f describes a curve similar to a linear arc, while the actuated joints reach values around $\theta_{1,5} > 50°$ and $\theta_{1,5} < -50°$ respectively. For the second scenario, Figure 4b, the input parameters are on hold, while the additional DoF is switched on. Then, due to the addition of a serial mechanism, the target flapping amplitude α includes the α_1 and α_2 angles.

The angle α_1 is implemented by Equation (21), which is related to the spatial mechanism, while the α_2 angle is implemented by Equation (26), which is associated with the serial mechanism. Thus, the target flapping amplitude α is described by:

$$\alpha = \alpha_1 + \alpha_2 \tag{27}$$

Here, $\alpha_1 = 0.4\alpha$, and $\alpha_2 = 0.6\alpha$. Additionally, for this simulation, $n = 3$, the vector $H = [34, 25, 35 + 296]$, and $\Psi = \alpha_2$. From Figure 4b, the change in the shape of the curve described by the fin's tip can be observed. It looks more similar to the natural manta ray movement, that is, the ∞ shape.

By comparing both scenarios, we found that the values computed for the actuated joints are lower when the third DoF is switched on: $\theta_{1,5} > 25°$ and $\theta_{1,5} < -25°$.

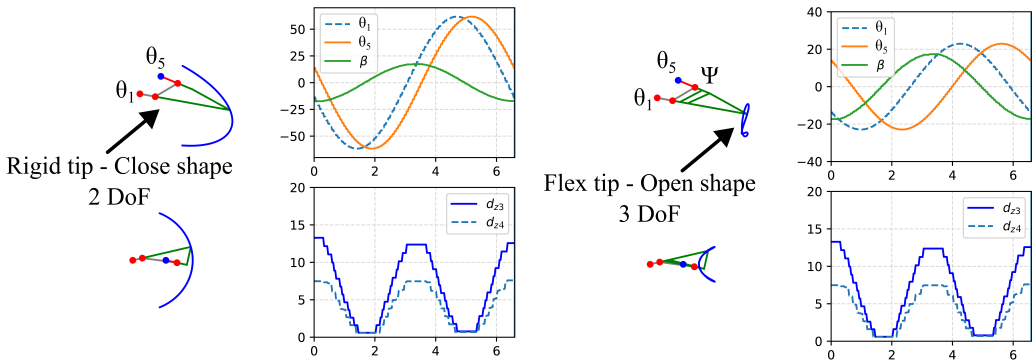

(**a**) (**b**)

Figure 4. Sinusoidal CPG input according to [5]. (**a**) Scenario 1: a literature approach with a 2 DoF fin mechanism. (**b**) Scenario 2: a mechanism with 3 DoFs, proposed by the authors.

3.2. Simulations Using a Natural Manta Ray Movement Approximation Approach

An approximation of a natural manta ray movement is defined by [10] as a relationship of two main variables defining the articulations trajectories as follows:

$$\begin{aligned} \alpha(t) = 206.7 \times \sin\left(0.037 \times \frac{60 \times (t+\phi)}{\pi} + 2.40\right) + \\ 176.3 \times \sin\left(0.033 \times \frac{60 \times (t+\phi)}{\pi} - 0.5\right) + \\ 10.07 \times \sin\left(0.098 \times \frac{60 \times (t+\phi)}{\pi} - 0.29\right) \end{aligned} \tag{28}$$

$$\beta(t) = 34.67 \times \sin\left(0.048 \times \frac{60 \times (t+\phi)}{\pi} + 1.073\right) + 9.08 \times \sin\left(0.107 \times \frac{60 \times (t+\phi)}{\pi} - 1.783\right) + 7.14 \times \sin\left(0.148 \times \frac{60 \times (t+\phi)}{\pi} - 2.41\right) \quad (29)$$

Equations (28) and (29) are considered for the fin mechanism simulation, taking into account the maximum pitching angle $\beta_{max} \leq 30°$ and the maximum flapping amplitude $\alpha_{max} \leq 60°$. However, due to the size discrepancy between a real manta ray and the prototype proposed, it is not possible to implement these input variables without modifying their amplitudes. Thus, the new pitching angle is $\beta_n = 0.7\beta(t)$, and the new flapping amplitude is $\alpha_n = 0.72\alpha(t)$ for the system without the third DoF.

In Figure 5, the simulation results derived from when the input signal can be given by Equations (28) and (29) are presented. Indeed, Figure 5a shows the performance of the fin mechanism when the third DoF is switched off. The curve described by the end-effector T_f is, again, shaped like a linear arc due to the fin stiffness. The parameters related to the actuated joints are similar to those obtained with the CPG approach: $-50° > \theta_{1,5} > 50°$.

For Scenario 4, the parameters selected for the simulation allow us to split the flapping amplitude between both mechanisms: $\alpha_1 = 0.3\alpha(t)$ and $\alpha_2 = 0.7\alpha(t)$. Due to the mechanism combination, it is not necessary create a new value for α_n.

Figure 5b shows the results for Scenario 4, that is, a scenario wherein the third DoF is switched on. The movement of the end-effector, T_f, describes an elliptic curve, mainly due to the system capacity, to split the flapping amplitude. Moreover, the parameters associated with active joints are lower than in Scenario 3, that is, $\theta_{1,5} > 25°$ and $\theta_{1,5} < -25°$.

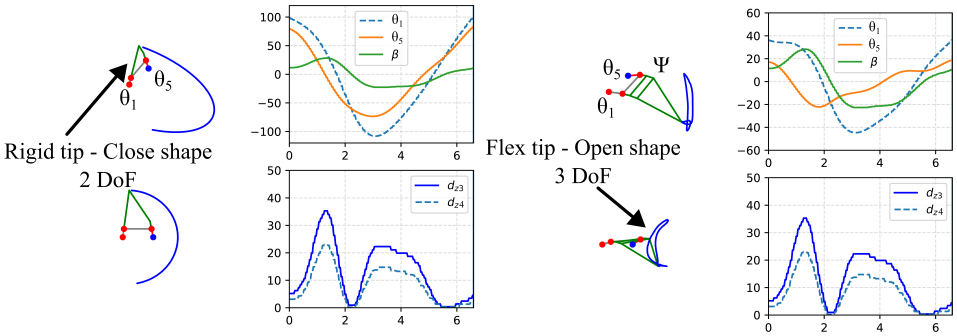

(**a**) (**b**)

Figure 5. Input signal according to [10]; manta ray natural movement; (**a**) Scenario 3: simulated movement with the third DoF switched off; (**b**) Scenario 4: the authors' proposed mechanism with the third DoF switched on.

4. Three-Dimensional Prototype of the Robotic Fin

Based on the kinematics analysis, the design of the robot is proposed as a combination of two systems to test the concept. The first system is a 2 DoF spatial mechanism, and the second system is a 1 DoF mechanism based on a cantilever beam with a middle compliant joint using layers of plastic materials; the hybrid mechanism decoupled is shown in Figure 6.

The main construction material used was acrylonitrile styrene acrylate (ASA), and construction was carried out using Fused Deposition Modeling (FDM) techniques for fabrication, while metallic parts were built using lathe techniques.

4.1. Prototype of 2 DoF Spatial Mechanism

Based on the design proposed by [5], a first prototype was designed to validate the movement. The design of the rear link was based on a commercial ball joint from SKF; this joint allows for a movement of 14° in all their axes. For the design of the lateral link, we

used a NACA0022 profile. However, this profile was modified to enhance the range of movement of the spherical joint. Additionally, due to the redundancy between cylindrical and spherical joints, it could be used to improve the workspace of the spherical joint.

Moreover, due to the size of the spherical joint body, a mechanical coupling was designed and manufactured to adapt the minimum distance between the lateral link base and the rear link (see Figure 6a).

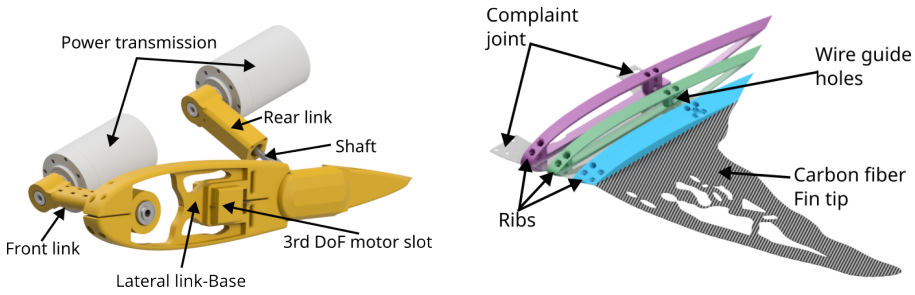

(**a**) (**b**)

Figure 6. Computer-Aided Design (CAD) description of the hybrid mechanism: (**a**) 3D model design proposed for the 2 DoF SPM; (**b**) proposed 3D model that is inclusive of the third DoF and based on a cantilever beam using compliant joints and wire to move it.

For this prototype, linear bearings, instead of friction bearings, were used due to blocking in the movements, lack of alignment, and the friction problems between the rear link and the rear shaft. In the lateral link, a compliant joint is placed at the 1 mm slot. It remains attached to the main body, and another slot is designed in order to insert a servomotor that transmits the power to the third degree of freedom (see Figure 6a).

4.2. Prototype of 1 DoF Mechanism

Despite the fact that, regarding the state of the art, it is possible to find previous research articles aimed at replicating manta ray movement, like [10,24,26], the main difference between our proposal and those previously reported lies in the actuation system of the additional DoF. Our mechanism was designed to be driven by wires. Then, the properties of plastic materials are used to emulate a compliant joint with four ribs, being part of the fin. The base, i.e., the lateral link base, with its curved-shape design, supports the forces applied to the wires.

For the real mechanism validation, a 1 mm polyethylene terephthalate glycol (PETG) sheet was selected; however, for real application, a thickener sheet will be used to prevent natural flexion due to the weight of the fin tip and the gravity forces applied on it. The shape selected covers the biggest area to support the weight of the entire mechanism. Despite the mechanism designed by [26] being 10 mm, our design is bigger due to the space between the base and the first rib.

Finally, the last part of the cantilever beam is made of a rigid carbon fiber the pattern of which replicates the fin shape. It is well known that carbon fiber material has good mechanical properties, such as stiffness and flexibility. The fin will be covered by a suitable skin made of polychloroprene or silicone.

The result of merging these two mechanisms is shown in Figure 7a.

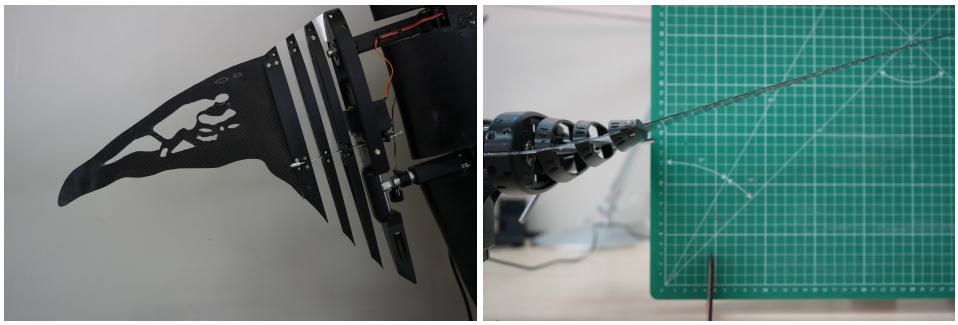

(**a**) (**b**)

Figure 7. Pictures of the developed fin prototype: (**a**) real prototype based on a hybrid robot. (**b**) Movement generated when applying the force described in the real prototype.

5. Discussion

In this paper, we have presented a new hybrid 3R-DoF mechanism aimed at replicating the natural movement of a manta ray fin. Despite similar approaches existing in the literature, our design introduces a novel aspect in the actuation system of the third DoF that is made by a wire that passes through ribs and pulls them up and down, and as consequence, the movement becomes soft because of this compliant joint. Additionally, the kinematics model was proposed under the Lie algebra method, which allows one to decouple the 3 DoF mechanism into two mechanisms, one with 2 DoFs and one with 1 DoF. After the implementation of the model in Matlab environments, several simulations were performed in order to compare the behaviour of the mechanisms proposed in the literature with 2 DoFs with our mechanism.

The natural undulatory movement was reproduced by a sinusoidal CPG. According to our results, the proposed mechanism improves the locomotion compared to those reported previously in the literature. Therefore, the 3R-DoF was designed and prototyped considering the hybrid mechanism SPM+compliant joint. Furthermore, the angle needed to obtain a full undulatory trajectory is lower. Taking into account the simulation results, it is possible to increase the autonomy of the robot due to the reduction in energy consumption by the actuators of the spatial parallel mechanism . On the other hand, manta rays have the ability to move in narrow spaces; this means that with the addition of the third DoF, it is possible to achieve high-performance maneuvers with small movements.

Kinematic analysis offers a deep understanding of how the addition of an extra DoF affects the whole mechanism. According to this, the transformation of α_{max} into α_1 and α_2 supposes a reduction in the angular displacements in the actuated joints, allowing for optimal values of movements, increasing the workspace.

Finally, we also conducted a study on whether the spherical joint mobility constraint affects the system movements and whether re-designing could increase the maximum pitching angle β_{max}.

6. Conclusions

In this paper, the design, prototyping, kinematics modeling, and simulation of a 3R-DoF hybrid mechanism was presented. The fin part of the manta ray underwater robot is currently under development. In this paper, we presented theoretical and simulation results that allow us to compare the performance of 2 DoF fin mechanisms, widely reported in the literature, and our mechanism, which was made with 3R-DoF and a compliant joint. The evidence presented demonstrates that the additional degree of freedom can contribute to improving the maneuverability and, at the same time, increase the autonomy of the underwater robot. Because the prototype was developed to turn the third DoF off or on, the next step is to carry out experiments in water to validate the advantages that the additional DoF provides to the robot.

Author Contributions: Conceptualization and writing—original draft, E.d.J.C.T. and C.E.G.C.; conceptual design, E.d.J.C.T. and C.E.G.C.; formal analysis, E.d.J.C.T. and L.E.G.G.; methodology, E.d.J.C.T. and C.E.G.C.; coding, E.d.J.C.T. and L.E.G.G.; simulation, E.d.J.C.T. and L.E.G.G.; results, E.d.J.C.T. and L.E.G.G.; figure creation, E.d.J.C.T.; validation, E.d.J.C.T. and L.E.G.G.; writing—reviewing and editing, E.d.J.C.T., L.E.G.G., L.E.V.M. and C.E.G.C.; funding acquisition, C.E.G.C. All authors have read and agreed to the published version of the manuscript.

Funding: This research was partially supported via a research project, Chair University-Industry Monodon, by Navantia Underwater Robots and Deeptech Technology. Reference id: CAT235618000.

Conflicts of Interest: The authors declare no conflicts of interest.

Abbreviations

The following abbreviations are used in this manuscript:

DoF	Degree of freedom
MPF	median and paired pectoral fin
SMA	shape memory alloy wire
SPM	spatial parallel mechanism
HTM	homogeneous transformation matrix
CM	global position
CPG	Central Pattern Generator
ASA	acrylonitrile styrene acrylate
FDM	Fused Deposition Modeling
CAD	Computer-Aided Design
PETG	polyethylene terephthalate glycol

References

1. Lam, K.; Tsui, T.; Nakano, K.; Randall, D.J. Physiological Adaptations of Fishes to Tropical Intertidal Environments. In *The Physiology of Tropical Fishes*; Fish Physiology; Academic Press: Cambridge, MA, USA, 2005; Volume 21; pp. 501–581. [CrossRef]
2. Wright, M.; Xiao, Q.; Dai, S.; Post, M.; Yue, H.; Sarkar, B. Design and development of modular magnetic bio-inspired autonomous underwater robot—MMBAUV. *Ocean Eng.* **2023**, *273*, 113968. [CrossRef]
3. Moored, K.W.; Fish, F.E.; Kemp, T.H.; Bart-Smith, H. Batoid fishes: Inspiration for the next generation of underwater robots. *Mar. Technol. Soc. J.* **2011**, *45*, 99–109. [CrossRef]
4. Burgess, K.B.; Couturier, L.I.; Marshall, A.D.; Richardson, A.J.; Weeks, S.J.; Bennett, M.B. *Manta birostris*, predator of the deep? Insight into the diet of the giant manta ray through stable isotope analysis. *R. Soc. Open Sci.* **2016**, *3*, 160717. [CrossRef] [PubMed]
5. Chen, L.; Bi, S.; Cai, Y.; Qiu, H. Design and Hydrodynamic Experiment Research on Novel Biomimetic Pectoral Fins of a Ray-Inspired Robotic Fish. *Machines* **2022**, *10*, 606. [CrossRef]
6. Zhou, C.; Low, K.H. Design and locomotion control of a biomimetic underwater vehicle with fin propulsion. *IEEE/ASME Trans. Mechatron.* **2012**, *17*, 25–35. [CrossRef]
7. Chen, L.; Bi, S.; Cai, Y.; Cao, Y.; Pan, G. Design and Experimental Research on a Bionic Robot Fish with Tri-Dimensional Soft Pectoral Fins Inspired by Cownose Ray. *J. Mar. Sci. Eng.* **2022**, *10*, 537. [CrossRef]
8. Low, K.H.; Seet, G.L.; Zhou, C. Biomimetic design and workspace study of compact and modular undulating fin body segments. In Proceedings of the 2007 IEEE International Conference on Mechatronics and Automation, ICMA 2007, Harbin, China, 5–8 August 2007; pp. 129–134. [CrossRef]
9. Cloitre, A.; Arensen, B.; Patrikalakis, N.M.; Youcef-Toumi, K.; Valdivia Y Alvarado, P. Propulsive performance of an underwater soft biomimetic batoid robot. In Proceedings of the International Offshore and Polar Engineering Conference, Busan, Republic of Korea, 15–20 June 2014; pp. 326–333.
10. Menzer, A.; Gong, Y.; Fish, F.E.; Dong, H. Bio-Inspired Propulsion: Towards Understanding the Role of Pectoral Fin Kinematics in Manta-like Swimming. *Biomimetics* **2022**, *7*, 45. [CrossRef] [PubMed]
11. Yurugi, M.; Shimanokami, M.; Nagai, T.; Shintake, J.; Ikemoto, Y. Cartilage structure increases swimming efficiency of underwater robots. *Sci. Rep.* **2021**, *11*, 11288. [CrossRef] [PubMed]
12. Takagi, K.; Yamamura, M.; Luo, Z.w.; Onishi, M.; Hirano, S.; Asaka, K.; Hayakawa, Y. Development of a Rajiform Swimming Robot using Ionic Polymer Artificial Muscles. In Proceedings of the 2006 IEEE/RSJ International Conference on Intelligent Robots and Systems, Beijing, China, 9–15 October 2006; pp. 1861–1866. [CrossRef]
13. Shin, S.R.; Migliori, B.; Miccoli, B.; Li, Y.C.; Mostafalu, P.; Seo, J.; Mandla, S.; Enrico, A.; Antona, S.; Sabarish, R.; et al. Electrically Driven Microengineered Bioinspired Soft Robots. *Adv. Mater.* **2018**, *30*, 1704189. [CrossRef] [PubMed]
14. Li, T.; Li, G.; Liang, Y.; Cheng, T.; Dai, J.; Yang, X.; Liu, B.; Zeng, Z.; Huang, Z.; Luo, Y.; et al. Fast-moving soft electronic fish. *Sci. Adv.* **2017**, *3*, e1602045. [CrossRef] [PubMed]

15. Wang, Z.; Wang, Y.; Li, J.; Hang, G. A micro biomimetic manta ray robot fish actuated by SMA. In Proceedings of the 2009 IEEE International Conference on Robotics and Biomimetics (ROBIO), Guilin, China, 19–23 December 2009; pp. 1809–1813. [CrossRef]
16. Liu, Y.; Chen, Z.; Chen, C.; Wang, T.; Tian, G.; Ji, S. Design of Bionic Manta Ray Driven by SMA. In Proceedings of the 2022 7th International Conference on Control and Robotics Engineering (ICCRE), Beijing, China, 15–17 April 2022; pp. 56–61. [CrossRef]
17. He, J.; Cao, Y.; Huang, Q.; Pan, G.; Dong, X.; Cao, Y. Effects of bionic pectoral fin rays' spanwise flexibility on forwarding propulsion performance. *J. Mar. Sci. Eng.* **2022**, *10*, 783. [CrossRef]
18. Sapmaz, A.R.; Dilibal, S.; Ozbaran, C.; Gercek, M. Development of Bioinspired Robotic Pectoral Fin Structure Using Radial Scissor Mechanism. In Proceedings of the HORA 2021—3rd International Congress on Human-Computer Interaction, Optimization and Robotic Applications, Ankara, Turkey, 11–13 June 2021; Institute of Electrical and Electronics Engineers Inc.: Piscataway, NJ, USA, 2021. [CrossRef]
19. Zhang, Y.; He, J.; Low, K.H. Parametric Study of an Underwater Finned Propulsor Inspired by Bluespotted Ray. *J. Bionic Eng.* **2012**, *9*, 166–176. [CrossRef]
20. Meng, Y.; Wu, Z.; Yu, J. Mechatronic Design of a Novel Robotic Manta with Pectoral Fins. In Proceedings of the 2019 IEEE 9th Annual International Conference on CYBER Technology in Automation, Control, and Intelligent Systems (CYBER), Suzhou, China, 29 July–2 August 2019; pp. 439–444. [CrossRef]
21. Zhang, Y.; Wang, S.; Wang, X.; Geng, Y. Design and Control of Bionic Manta Ray Robot with Flexible Pectoral Fin. In Proceedings of the IEEE International Conference on Control and Automation, ICCA, Anchorage, AK, USA, 12–15 June 2018; IEEE Computer Society: Washington, DC, USA, 2018, Volume 2018; pp. 1034–1039. [CrossRef]
22. Fisheries, N. Giant Manta Ray, 2023. Available online: https://www.fisheries.noaa.gov/species/giant-manta-ray (accessed on 10 July 2024).
23. Marinewise. Giant Manta Ray-Manta Birostris, 2022. Available online: https://marinewise.com.au/shark-and-ray-species/giant-manta-ray/ (accessed on 10 July 2024)
24. Lu, Y.; Meng, S.; Xing, C.; Hao, Y.; Cao, Y.; Pan, G.; Cao, Y. Effect of Active–Passive Deformation on the Thrust by the Pectoral Fins of Bionic Manta Robot. *J. Bionic Eng.* **2024**, *21*, 718–728. [CrossRef]
25. Yime, E.; Saltarén, R.J.; Mckinley, J.A.R. Análisis dinámico inverso de robots paralelos: Un tutorial con álgebra de Lie. *Rev. Iberoam. Automática E Informática Ind.* **2023**, *20*, 327–346. [CrossRef]
26. van den Berg, S.C.; Scharff, R.B.; Rusák, Z.; Wu, J. OpenFish: Biomimetic design of a soft robotic fish for high speed locomotion. *HardwareX* **2022**, *12*, e00320. [CrossRef]